






Article

X-Ray Absorption Spectroscopy Measurements of Cu-ProIAPP Complexes at Physiological Concentrations

Emiliano De Santis ^{1,2}, Emma Shardlow ³, Francesco Stellato ^{2,*}, Olivier Proux ⁴,
Giancarlo Rossi ^{1,2,5}, Christopher Exley ³ and Silvia Morante ^{1,2}

¹ Dipartimento di Fisica, Università di Roma "Tor Vergata", Via della Ricerca Scientifica, I-00133 Roma, Italy; edesantis@roma2.infn.it (E.D.S.); rossi@roma2.infn.it (G.R.); morante@roma2.infn.it (S.M.)

² Istituto Nazionale di Fisica Nucleare (INFN), Sezione di Roma 2, Via della Ricerca Scientifica, I-00133 Roma, Italy

³ The Birchall Centre, Lennard-Jones Laboratories, Keele University, Staffordshire ST5 5BG, UK; e.shardlow@keele.ac.uk (E.S.); c.exley@keele.ac.uk (C.E.)

⁴ Observatoire des Sciences de l'Univers de Grenoble, UMS 832 CNRS-Université Grenoble Alpes, 38041 Grenoble, France; olivier.proux@esrf.fr

⁵ Centro Fermi-Museo Storico della Fisica e Centro Studi e Ricerche "Enrico Fermi", 00184 Roma, Italy

* Correspondence: francesco.stellato@roma2.infn.it

Received: 12 December 2018; Accepted: 15 January 2019; Published: 18 January 2019



Abstract: The amyloidogenic islet amyloid polypeptide (IAPP) and the associated pro-peptide ProIAPP_{1–48} are involved in cell death in type 2 diabetes mellitus. It has been observed that interactions of this peptide with metal ions have an impact on the cytotoxicity of the peptides as well as on their deposition in the form of amyloid fibrils. In particular, Cu(II) seems to inhibit amyloid fibril formation, thus suggesting that Cu homeostasis imbalance may be involved in the pathogenesis of type 2 diabetes mellitus. We performed X-ray Absorption Spectroscopy (XAS) measurements of Cu(II)-ProIAPP complexes under near-physiological (10 μM), equimolar concentrations of Cu(II) and peptide. Such low concentrations were made accessible to XAS measurements owing to the use of the High Energy Resolved Fluorescence Detection XAS facility recently installed at the ESRF beamline BM16 (FAME-UHD). Our preliminary data show that XAS measurements at micromolar concentrations are feasible and confirm that ProIAPP_{1–48}-Cu(II) binding at near-physiological conditions can be detected.

Keywords: X-ray absorption spectroscopy; amylin; high energy resolution fluorescence detection

1. Introduction

Type 2 diabetes mellitus (T2DM) is one of the most common chronic diseases, affecting over 300 million people worldwide. Amylin or Islet Amyloid PolyPeptide (IAPP), is a peptide composed of 37 amino acids that was first discovered as a constituent of amyloid deposits in the islets of Langerhans in individuals diagnosed with diabetes [1]. IAPP is highly amyloidogenic and it is this property that implicates it in the degeneration of islet β cells in diabetes [2]. The precursor to IAPP is the 67 amino acid peptide ProIAPP that upon incomplete processing leads to ProIAPP_{1–48} that has also been found in amyloid deposits in diabetes [3]. Recent research implicates aberrant or incomplete processing of ProIAPP in the aetiology of diabetes [4].

While both IAPP and ProIAPP_{1–48} readily form amyloids in vitro, their in vivo concentration is significantly below saturation and a burgeoning body of research is investigating this conundrum [5]. The aggregation of super-saturated concentrations of IAPP is influenced by aluminium [6,7], iron [7], zinc [7,8] and copper [7]. It remains equivocal as to whether Al(III), Fe(III) and Zn(II) promote amyloid

(β sheet) formation while it is clear that Cu(II) prevents IAPP from assembling into β -sheet structures [7] as recently confirmed [9–13]. ProIAPP_{1–48} forms amyloid less readily than IAPP and while there are few data on its interactions with metals it is also the case that Cu(II) prevents ProIAPP_{1–48} from forming β -sheets structures more prone to amyloidogenesis [12,14,15]. A sketch of the process leading to the formation of ProIAPP_{1–48} and IAPP and of their effect on islet β cells is depicted in Figure 1.

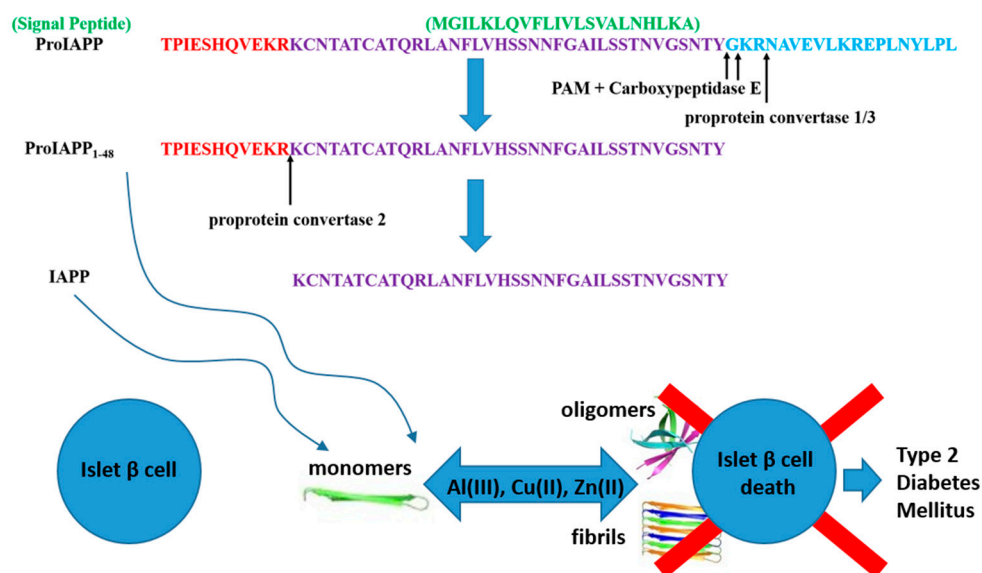


Figure 1. In the top part of the figure the amino acid sequences of ProIAPP, ProIAPP_{1–48} and IAPP are given. In the bottom part we sketch the path leading to β cells death (hence to T2DM) as a consequence of fibrillation processes of ProIAPP_{1–48} and IAPP monomers promoted by metal ions.

It is widely believed that the cytotoxicity of IAPP and ProIAPP_{1–48} is related to their propensity to form toxic oligomers during the early stages of amyloid formation [4] and it has been suggested that metals and specifically Cu(II) potentiate toxicity through stabilisation of these oligomeric forms [12,16].

It appears therefore to be of the utmost biological and, in perspective, medical importance, to unravel the detailed interaction mechanism between metal ions and amyloidogenic islet peptides. X-ray Absorption Spectroscopy (XAS) is the technique of election to selectively obtain, at atomic resolution, information about the metals environment even in the non-crystalline systems of biological interest. Indeed, XAS has been proven to be particularly useful for the study of the metal binding mode in a number of cases related to amyloidogenic proteins [17–20].

As recalled above, both IAPP and ProIAPP_{1–48} form amyloids *in vitro* but their typical concentration *in vivo* is significantly lower than the one used in *in vitro* experiments [21]. Since the behaviour of these peptides in the presence of metal ions does not only depend on the metal/peptide concentration ratio but can also be influenced by their absolute concentration, it is important to perform experiments as close as possible to the physiological conditions. This means that we need to perform experiments in systems where the metal concentration is in the micromolar range.

To tackle the severe signal-to-noise ratio problem associated with such low concentrations, we took advantage of the possibilities offered by the recently installed High Energy Resolved Fluorescence Detection (HERFD) XAS line, operational at the FAME-UHD beamline at ESRF (Grenoble, France) [22]. The interesting features of this high resolution XAS measurement scheme have already been successfully used to study biological samples, such as Fe-containing systems [23], Mo K-edge XAS in nitrogenase [24], the binuclear Fe centre in hydrogenase [25] and Cu organic compounds [26]. Other methods such as X-ray Emission Spectroscopy can be implemented easily using this kind of high resolution measurement, with great interest in the studies of metalloproteins [27].

With this work we pushed the limits of the technique to the study of ultra-highly diluted metal-protein complexes. The qualitative, biologically significant results we show on the metal-ProIAPP complexes are therefore intended to exhibit the potential of the HERFD-XAS technique in this context.

2. Materials and Methods

ProIAPP₁₋₄₈ fragments were synthesised using an Applied Biosystems 433A peptide synthesiser through the application of standard Fmoc-based solid phase methodology. The peptide amino acid sequence is TPIESHQVEKRKCNATCATQRLANFLVHSSNNGAILSSSTNVGSNTY. It is worth recalling that the ProIAPP₁₋₄₈ fragment is an intermediate form in the process that leads to the formation of the 37 residues long IAPP from the 67 amino acid long ProIAPP. A schematic view of the proteolytic cleavages that lead to the formation of ProIAPP₁₋₄₈ and IAPP is given in Figure 1.

Purification of the peptide was performed with the help of RP HPLC on a POROS 20R2 column using water/acetonitrile mixtures buffered with 0.1% TFA. The peptide content of the purified material (77%) was determined by quantitative amino acid analysis and lyophilised aliquots were stored at $-80\text{ }^{\circ}\text{C}$ prior to the preparation of peptide stock solutions. Peptide stocks were prepared to a final concentration of *ca* 150 μM via the addition of ultrapure water ($<0.067\text{ }\mu\text{S}/\text{cm}$) to thawed peptide lyophilisates. This stock was then used to prepare smaller individual volumes of the peptide in order to achieve the final concentrations of peptide included in the following experiments and these aliquots were stored at $-20\text{ }^{\circ}\text{C}$ until required. Thawed peptide aliquots were introduced into modified Krebs-Henseleit (KH) buffers ($\text{pH } 7.4 \pm 0.05$) [12] with or without the respective metals (added from certified stocks (Perkin-Elmer) at the required total metal concentrations to give final peptide concentration of 10 μM).

Sub-stoichiometric, 9 μM Cu(II) ions are added thus minimizing the amount of free Cu(II) in solution. In order to investigate the effect on the Cu(II) binding mode of the presence of other metals, like Al(III) and Zn(II) ions at different concentrations, we added the second metal at a concentration of either 50 or 1500 μM . Including Cu(II) in buffer as a blank. In all we have prepared and subjected to XAS measurements the six samples listed in Table 1.

Table 1. List of the measured samples. Sample name is given in column 1, peptide concentration in column 2, Cu, Zn and Al concentrations in columns 3, 4 and 5, respectively.

Sample(μM)	[Peptide] (μM)	[Cu] (μM)	[Zn] (μM)	[Al] (μM)
Cu buffer	0	1600	0	0
Cu-ProIAPP ₁₋₄₈	10	9	0	0
(Cu + Zn ^{Low})-ProIAPP ₁₋₄₈	10	9	50	0
(Cu + Al ^{Low})-ProIAPP ₁₋₄₈	10	9	0	50
(Cu + Zn ^{High})-ProIAPP ₁₋₄₈	10	9	1500	0
(Cu + Al ^{High})-ProIAPP ₁₋₄₈	10	9	0	1500

Copper K-edge (8.979 keV) XANES measurements were performed on the BM16 beamline (CRG FAME-UHD) at the ESRF (Grenoble, France) [22]. The main optical elements of the beamline were a two-crystal Si(220) monochromator located between two Rh-coated mirrors. The beam size on the sample was around $200 \times 100\text{ }\mu\text{m}^2$ ($H \times V$, FWHM) thanks to the sagittal focus of the 2nd crystal of the monochromator and the vertical one of the 2nd mirror. The 1st crystal of the monochromator is liquid nitrogen cooled in order to limit its thermal bump due to the incoming photons thus increasing the energy resolution of the monochromatic beam. Energy calibration was done by setting the 1st maximum of the 1st derivative of the copper metallic foil absorption spectrum to 8.979 keV. A 5-crystal analyser spectrometer on a Johann-type geometry (Figure 2), equipped with Si(444) bent crystals with a 1m radius of curvature (from Crystal Analyser Laboratories, ESRF) was used for fluorescence detection. The spectrometer was aligned so as to have the crystals in Bragg conditions at the Cu $K_{\alpha 1}$ emission line photons energy. The overall instrument energy resolution (combining crystal analyser

spectrometer and monochromator contributions) was established to be 0.7 eV by measuring the full width at half maximum of the elastic peak (measured by scanning the incident photon energy, with the monochromator, across the fluorescence photon energy, selected by the spectrometer). All the photons scattered by the crystals were collected using an energy-resolved silicon-drift detector, which allows discriminating the diffracted photons of interest from the other scattered ones.

For a typical biological system, in which the total radiation background (including elastic and inelastic scattering) is substantially more intense than the fluorescence line of interest, the advantage of background removal associated to the HERFD-XAS data acquisition scheme outweighs the disadvantage of having a lower total signal intensity with respect to a standard XAS measuring apparatus, such as a solid-state detector. XAS measurements of samples as diluted as those of interest here are made possible thanks to the use of this set-up that, significantly improve the signal-to-noise ratio, thus allowing nearly background-free measurements.

Data acquisition was performed using a liquid helium cryostat in order to limit sample evolution due to radiation damage under the beam.

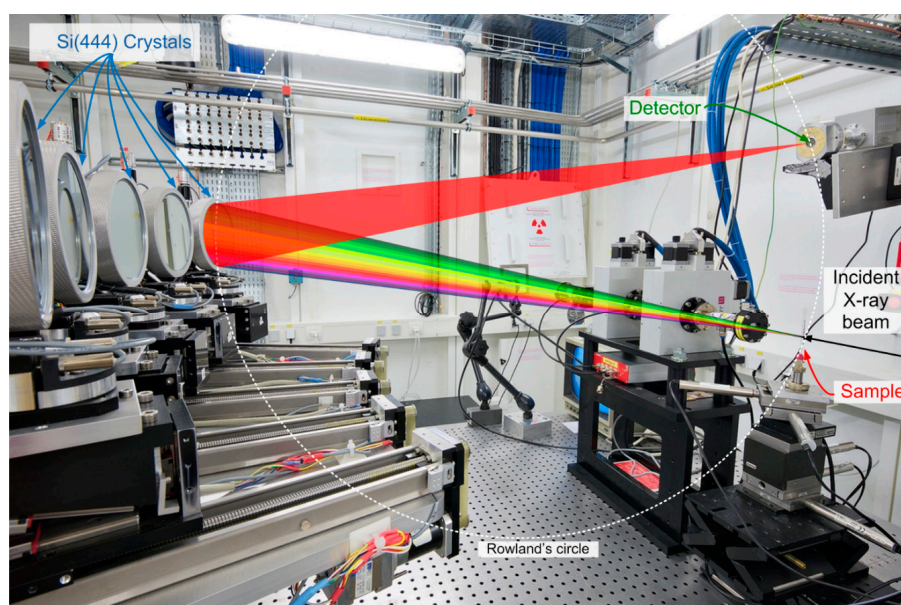


Figure 2. A picture of the FAME UHD beamline showing the HERFD acquisition geometry. In Johann geometry the sample, crystal centre and detector are on the Rowland's circle. The diameter of this circle is equal to the curvature radius of the crystals. A polyurethane balloon filled with He gas was placed between the sample, the crystals and the detector in order to minimize the air absorption of the fluorescence photons along the sample-crystal-detector path.

3. Results and Discussion

Cu K-edge XANES spectra of the sample listed in Table 1 are all gathered in Figure 3. Spectra of the Cu-ProIAPP₁₋₄₈ samples appear to be rather noisy but one has to keep in mind that Cu is present at the extremely low concentration of 9 μM (that corresponds to 0.6 ppm). To the best of our knowledge this is the first time in which XAS measurements are performed to probe the copper speciation in biological systems at bio-relevant concentration.

In the Figure 3, we compare the XANES spectrum of the Cu-ProIAPP₁₋₄₈ sample in the absence and in the presence of either Al(III) or Zn(II) ions at two different concentrations, namely 50 μM and 1500 μM , with the idea of detecting possible modifications of the Cu binding mode upon adding a second metal.

The XANES spectrum of Cu in buffer displays features typical of hydrated copper [28], while the XANES spectrum of Cu-ProIAPP₁₋₄₈ has a significantly different shape, indicating that Cu is bound to

ProIAPP₁₋₄₈. The Cu-ProIAPP₁₋₄₈ spectrum has an absorption maximum at nearly the same position as Cu in buffer, confirming that copper, as expected, is in its doubly ionized form, Cu(II).

It is interesting to note that Zn(II) and Al(III) added in solution seem to affect the Cu-ProIAPP₁₋₄₈ coordination mode in a way that depends on their concentration. In particular Zn(II) is seen to affect the XANES spectrum of Cu-ProIAPP₁₋₄₈ at high (black line), while Al(III) at low (light blue line) concentration.

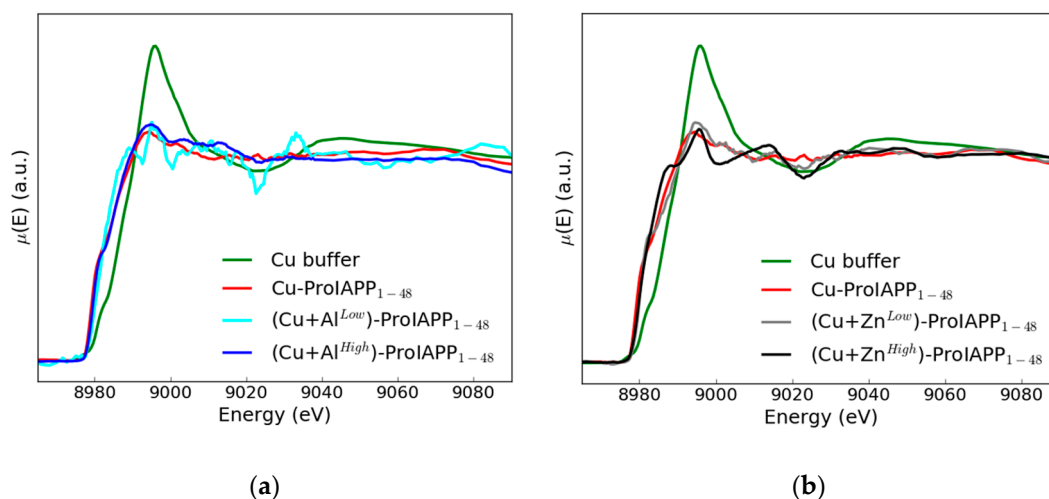


Figure 3. The XANES spectra of the Cu-buffer (green line) and Cu-ProIAPP₁₋₄₈ sample in the absence of metal ions (red line) compared in panel (a) with the Cu-ProIAPP₁₋₄₈ spectrum in the presence of 50 μ M Al(III) (light blue line) and 1500 μ M Al(III) (blue line) and in panel (b) in the presence of 50 μ M Zn(II) (grey line) and 1500 μ M Zn(II) (black line).

These qualitative findings are supported by Thioflavine T (ThT) fluorescence and Dynamic Light Scattering (DLS) measurements. In Reference [14], some of the authors of the present paper observed that, at a ProIAPP₁₋₄₈ concentration of 20 μ M, which is close to the one of the present study, the peptide forms ThT-fluorescence positive aggregates. In the presence of an equimolar concentration of Cu(II), the ThT-fluorescence is instead significantly reduced. In reference [21] they perform DLS measurements showing that Cu(II) has an effect on ProIAPP₁₋₄₈ aggregation in the direction of increasing the average aggregate size. The results of the experiments presented here confirm these observations and demonstrate that the effect of Cu(II) on ProIAPP₁₋₄₈ fibrillization is due to a direct binding between the Cu(II) ions and the peptide.

For what concerns the role of other metal ions, in Reference [21] the same authors show that Al(III) at equimolar concentration with the peptide does not have a detectable effect on ProIAPP₁₋₄₈ aggregate size. Although the ProIAPP₁₋₄₈ concentrations considered in Reference [21] were higher (5–60 μ M) than that used in this study, this observation is in agreement with what we observe here, namely that at low concentrations Al(III) ions do not have significant effects. Moreover, in Reference [14] it was also observed that the ThT fluorescence of 20 μ M ProIAPP₁₋₄₈ was unaffected by the presence of 10-fold excess of Zn(II) ion, while the fluorescence was significantly lower in the presence of an additional 10 μ M Cu(II). Although these measurements are not performed in exactly the same conditions as in the present study, taken all together they contribute to form a picture in which Cu(II) most strongly affects ProIAPP₁₋₄₈ aggregation, with Al(III) and Zn(II) being able to modulate its effect.

4. Conclusions

We are well aware of the fact that the quality of the collected spectra does not allow any speculation about the structural differences of the possible different Cu(II) coordination modes induced by the presence of Al(III) or Zn(II). Nevertheless, we think that the results we obtained are relevant in two respects.

1. Though yet at a qualitative level, the existence of differences in the XANES spectral features induced by the presence of the Zn(II) or Al(III) in the Cu(II)-ProIAPP_{1–48} binding mode sample is clearly established. These differences appear to be dependent (in different way) from the added ion concentration.
2. Experiments of the kind we have been able to perform at the ESRF HERFD XAS line demonstrate the general feasibility of XAS measurements on samples where the absorbing atom is present at micromolar concentration. This last fact is of special methodological relevance as it shows that it is possible to perform XAS measurements on very diluted metal-peptide complexes in physiological conditions, when raising metal ions concentration to improve the signal-to-noise ratio is not possible, as this would dramatically alter their physiological coordination mode.

In this paper we have successfully demonstrated the feasibility of XAS measurements of very diluted samples (i.e., where the absorber concentration is at the micromolar level) and proved that adding in solution either Zn(II) or Al(III) has a detectable impact on the Cu coordination. If, as a next step, one wants to arrive at a detailed description of the Cu(II)-ProIAPP_{1–48} coordination mode, some kind of information about the metal site structure is required. To this end NMR, X-ray crystallography and numerical (classical and/or, *ab initio*) molecular approaches could be of much help, as demonstrated in the study of similar instances performed in References [28,29].

Concluding we would like to stress that XAS is an invaluable and irreplaceable tool when the interest is to get highly resolved (order of hundredths of Angstrom) structural information on the metal site even for very diluted samples like the ones one often finds in the case of biological systems in physiological conditions. Neither NMR (that needs isotopic labelling) nor X-ray diffraction (that requires crystals) are as informative and easily accessible as XAS in these circumstances. This point is largely acknowledged by people working in experimental groups that routinely use NMR and X-ray diffraction. Indeed, when available, NMR and/or X-ray diffraction data are often refined (confirmed) with complementary XAS measurements [30–34].

Author Contributions: Sample preparation: E.S. and C.E.; data acquisition: S.M., O.P. and F.S.; data analysis: E.D.S., S.M., O.P., G.R. and F.S.; writing: C.E., S.M., O.P., G.R., E.S. and F.S.

Funding: This work was partly supported by INAIL grant BRiC 2016 ID17/2016 and by INFN CIPE grant HPC_HTC 14064. Construction of the 5 crystals spectrometer used on BM16/FAME-UHD for this experiment was financially supported by the French National Institute for Earth Science and Astronomy of the CNRS (INSU CNRS), ANR NANOSURF (coordinator: C. Chaneac, LCMCP), ANR MESONNET (coordinator: J.Y. Bottero, CEREGE), CEREGE laboratory (Aix en Provence, France) and Labex OSUG@2020 (ANR-10-LABX-0056). The FAME-UHD project is financially supported by the French “invest for the future” EquipEx (EcoX, ANR-10-EQPX-27-01), the CEA-CNRS CRG consortium and the French National Institute for Earth Science and Astronomy of the CNRS (INSU CNRS).

Conflicts of Interest: The authors declare no conflict of interest.

References

1. Cooper, G.J.; Willis, A.C.; Clark, A.; Turner, R.C.; Sim, R.B.; Reid, K.B. Purification and characterization of a peptide from amyloid-rich pancreases of type 2 diabetic patients. *Proc. Natl. Acad. Sci. USA* **1987**, *84*, 8628–8632. [[CrossRef](#)] [[PubMed](#)]
2. Konarkowska, B.; Aitken, J.F.; Kistler, J.; Zhang, S.G.; Cooper, J. The aggregation potential of human amylin determines its cytotoxicity towards islet beta-cells. *FEBS J.* **2006**, *273*, 3614–3624. [[CrossRef](#)] [[PubMed](#)]
3. Westermark, P.; Engstrom, U.; Westermark, G.T.; Johnson, K.H.; Permerth, J.; Betsholtz, C. Islet amyloid polypeptide (IAPP) and pro-IAPP immunoreactivity in human islets of Langerhans. *Diabetes Res. Clin. Pract.* **1989**, *7*, 219–226. [[CrossRef](#)]
4. Courtade, J.A.; Klimek-Abercrombie, A.M.; Chen, Y.-C.; Patel, N.; Lu, P.Y.T.; Speake, C.; Orban, P.C.; Najafian, B.; Meneilly, G.; Greenbaum, C.J.; et al. Measurement of pro-islet amyloid polypeptide (1–48) in diabetes and islet transplants. *J. Clin. Endocrinol. Metab.* **2017**, *102*, 2595–2603. [[CrossRef](#)] [[PubMed](#)]
5. Raleigh, D.; Zhang, X.; Hastoy, B.; Clark, A. The β -cell assassin: IAPP cytotoxicity. *J. Mol. Endocrinol.* **2017**, *59*, R121–R140. [[CrossRef](#)] [[PubMed](#)]

6. Exley, C.; Korchazhkina, O. Promotion of formation of amyloid fibrils by aluminium adenosine triphosphate (AlATP). *J. Inorg. Biochem.* **2001**, *84*, 215–224. [[CrossRef](#)]
7. Ward, B.; Walker, K.; Exley, C. Cu(II) inhibits the formation of amylin amyloid in vitro. *J. Inorg. Biochem.* **2008**, *102*, 371–375. [[CrossRef](#)]
8. Brender, J.R.; Hartman, K.; Nanga, R.P.R.; Popovych, N.; Bea, R.D.; Vivekanandan, S.; Marsh, E.G.N.; Ramamoorthy, A. Role of zinc in human islet amyloid polypeptide aggregation. *J. Am. Chem. Soc.* **2010**, *132*, 8973–8983. [[CrossRef](#)]
9. Ma, L.; Li, X.; Wang, Y.; Zheng, W.; Chen, T. Cu(II) inhibits hIAPP fibrillation and promotes hIAPP-induced beta cell apoptosis through induction of ROS-mediated mitochondrial dysfunction. *J. Inorg. Biochem.* **2014**, *140*, 143–152. [[CrossRef](#)]
10. Li, H.; Ha, E.; Donaldson, R.P.; Jeremic, A.M.; Vertes, A. Rapid assessment of human amylin aggregation and its inhibition by copper (II) ions by laser ablation electrospray ionisation mass spectrometry with ion mobility separation. *Anal. Chem.* **2015**, *87*, 9829–9837. [[CrossRef](#)]
11. Riba, I.; Barran, P.E.; Cooper, G.J.S.; Unwin, R.D. On the structure of the copper-amylin complex. *Int. J. Mass Spectrom.* **2015**, *391*, 47–53. [[CrossRef](#)]
12. Mold, M.; Bunrat, C.; Goswami, P.; Roberts, A.; Roberts, C.; Taylor, N.; Taylor, H.; Wu, L.; Fraser, P.E.; Exley, C. Further insight into the role of metals in amyloid formation by IAPP_{1–37} and ProIAPP_{1–48}. *J. Diabetes Res. Clin. Metab.* **2015**, *4*. [[CrossRef](#)]
13. Sánchez-López, C.; Cortés-Mejía, R.; Miotto, M.C.; Binolfi, A.; Fernández, C.O.; del Campo, J.M.; Quintanar, L. Copper coordination features of human islet amyloid polypeptide: The type 2 diabetes peptide. *Inorg. Chem.* **2016**, *55*, 10727–10740. [[CrossRef](#)]
14. Exley, C.; House, E.; Patel, T.; Wu, L.; Fraser, P.E. Human pro-islet amyloid polypeptide (ProIAPP_{1–48}) forms amyloid fibrils and amyloid spherulites in vitro. *J. Inorg. Biochem.* **2010**, *104*, 1125–1129. [[CrossRef](#)] [[PubMed](#)]
15. Exley, C.; Mold, M.; Shardlow, E.; Shuker, B.; Ikpe, B.; Wu, L.; Fraser, P.E. Copper is a potent inhibitor of the propensity for human ProIAPP_{1–48} to form amyloid fibrils in vitro. *J. Diabetes Res. Clin. Metab.* **2012**, *1*, 3. [[CrossRef](#)]
16. Lee, S.J.C.; Choi, T.S.; Lee, J.W.; Lee, H.J.; Mun, D.-G.; Akashi, S.; Lee, S.-W.; Lim, M.H.; Kim, H.I. Structure and assembly mechanisms of toxic human islet amyloid polypeptide oligomers associated with copper. *Chem. Sci.* **2016**, *7*, 5398–5406. [[CrossRef](#)] [[PubMed](#)]
17. De Santis, E.; Minicozzi, V.; Proux, O.; Rossi, G.C.; Silva, K.I.; Lawless, M.J.; Stellato, F.; Saxena, S.; Morante, S. Cu(II)–Zn(II) Cross-Modulation in Amyloid–Beta Peptide Binding: An X-ray Absorption Spectroscopy Study. *J. Phys. Chem. B* **2015**, *119*, 15813–15820. [[CrossRef](#)]
18. Stellato, F.; Spevacek, A.; Proux, O.; Minicozzi, V.; Millhauser, G.; Morante, S. Zinc modulates copper coordination mode in prion protein octa-repeat subdomains. *Eur. Biophys. J.* **2011**, *40*, 1259–1270. [[CrossRef](#)]
19. Stellato, F.; Minicozzi, V.; Millhauser, G.L.; Pascucci, M.; Proux, O.; Rossi, G.C.; Morante, S. Copper–zinc cross-modulation in prion protein binding. *Eur. Biophys. J.* **2014**, *43*, 631–642. [[CrossRef](#)]
20. Stellato, F.; Fusco, Z.; Chiaraluce, R.; Consalvi, V.; Dinarelli, S.; Placidi, E.; Petrosino, M.; Rossi, G.C.R.; Minicozzi, V.; Morante, S. The effect of β -sheet breaker peptides on metal associated Amyloid- β peptide aggregation process. *Biophys. Chem.* **2017**, *229*, 110–114. [[CrossRef](#)]
21. Shardlow, E.; Rao, C.; Sattarov, R.; Wu, L.; Fraser, P.E.; Exley, C. Aggregation of the diabetes-related peptide ProIAPP_{1–48} measured by dynamic light scattering. *J. Trace Elem. Med. Biol.* **2019**, *51*, 1–8. [[CrossRef](#)] [[PubMed](#)]
22. Proux, O.; Lahera, E.; Del Net, W.; Kieffer, I.; Rovezzi, M.; Testemale, D.; Irar, M.; Thomas, S.; Aguilar-Tapia, A.; Bazarkina, E.F.; et al. High-energy resolution fluorescence detected X-ray absorption spectroscopy: A powerful new structural tool in environmental biogeochemistry sciences. *J. Environ. Qual.* **2017**, *46*, 1146–1157. [[CrossRef](#)] [[PubMed](#)]
23. Castillo, R.G.; Banerjee, R.; Allpress, C.J.; Rohde, G.T.; Bill, E.; Que, L., Jr.; Lipscomb, J.D.; DeBeer, S. High-energy-resolution fluorescence-detected X-ray absorption of the Q intermediate of soluble methane monooxygenase. *JACS* **2017**, *139*, 18024–18033. [[CrossRef](#)] [[PubMed](#)]
24. Bjornsson, R.; Lima, F.A.; Spatzal, T.; Weyhermüller, T.; Glatzel, P.; Bill, E.; Einzle, O.; Neese, F.; DeBeer, S. Identification of a spin-coupled Mo(III) in the nitrogenase iron–molybdenum cofactor. *Chem. Sci.* **2014**, *5*, 3096–3103. [[CrossRef](#)]

25. Mebs, S.; Kositzki, R.; Duan, J.; Kertess, L.; Senger, M.; Wittkamp, F.; Apfel, U.P.; Happe, T.; Stripp, S.T.; Winkler, M.; et al. Hydrogen and oxygen trapping at the H-cluster of [FeFe]-hydrogenase revealed by site-selective spectroscopy and QM/MM calculations. *Biochim. Biophys. Acta Bioenerg.* **2018**, *1859*, 28–41. [[CrossRef](#)] [[PubMed](#)]
26. Vollmers, N.J.; Müller, P.; Hoffmann, A.; Herres-Pawlis, S.; Rohrmüller, M.; Schmidt, W.G.; Gerstmann, U.; Bauer, M. Experimental and theoretical high-energy-resolution X-ray absorption spectroscopy: Implications for the investigation of the entatic state. *Inorg. Chem.* **2016**, *55*, 11694–11706. [[CrossRef](#)] [[PubMed](#)]
27. Kowalska, J.K.; Lima, F.A.; Pollock, C.J.; Rees, J.A.; DeBeer, S. A practical guide to high-resolution X-ray spectroscopic measurements and their applications in bioinorganic chemistry. *Isr. J. Chem.* **2016**, *56*, 803–815. [[CrossRef](#)]
28. La Penna, G.; Minicozzi, V.; Morante, S.; Rossi, G.C.; Stellato, F. A first-principle calculation of the XANES spectrum of Cu²⁺ in water. *J. Chem. Phys.* **2015**, *143*, 124508. [[CrossRef](#)] [[PubMed](#)]
29. Stellato, F.; Calandra, M.; D’Acapito, F.; De Santis, E.; La Penna, G.; Rossi, G.C.; Morante, S. Multi-scale theoretical approach to X-ray absorption spectra in disordered systems: An application to the study of Zn(II) in water. *Phys. Chem. Chem. Phys.* **2018**, *20*, 24775–24782. [[CrossRef](#)] [[PubMed](#)]
30. Banci, L.; Bertini, I.; Mangani, S. Integration of XAS and NMR techniques for the structure determination of metalloproteins. Examples from the study of copper transport proteins. *J. Synchrotron Radiat.* **2005**, *12*, 94–97. [[CrossRef](#)]
31. Koutmou, K.S.; Casiano-Negroni, A.; Getz, M.M.; Pazicni, S.; Andrews, A.J.; Penner-Hahn, J.E.; Al-Hashimi, H.M.; Fierke, C.A. NMR and XAS reveal an inner-sphere metal binding site in the P4 helix of the metallo-ribozyme ribonuclease P. *Proc. Natl. Acad. Sci. USA* **2010**, *107*, 2479–2484. [[CrossRef](#)] [[PubMed](#)]
32. Arcovito, A.; Moschetti, T.; D’Angelo, P.; Mancini, G.; Vallone, B.; Brunori, M.; Della Longa, S. An X-ray diffraction and X-ray absorption spectroscopy joint study of neuroglobin. *Arch. Biochem. Biophys.* **2008**, *475*, 7–13. [[CrossRef](#)] [[PubMed](#)]
33. Frankær, C.G.; Knudsen, M.V.; Norén, K.; Nazarenko, E.; Ståhl, K.; Harris, P. The structures of T6, T3R3 and R6 bovine insulin: Combining X-ray diffraction and absorption spectroscopy. *Acta Crystallogr. D* **2012**, *68*, 1259–1271. [[CrossRef](#)] [[PubMed](#)]
34. Koebke, K.J.; Ruckthong, L.; Meagher, J.L.; Mathieu, E.; Harland, J.; Deb, A.; Lehnert, N.; Policar, C.; Tard, C.; Penner-Han, J.E.; et al. Clarifying the Copper Coordination Environment in a de Novo Designed Red Copper Protein. *Inorg. Chem.* **2018**, *57*, 12291–12302. [[CrossRef](#)] [[PubMed](#)]



© 2019 by the authors. Licensee MDPI, Basel, Switzerland. This article is an open access article distributed under the terms and conditions of the Creative Commons Attribution (CC BY) license (<http://creativecommons.org/licenses/by/4.0/>).